EPIC2001 AND THE COUPLED OCEAN–ATMOSPHERE SYSTEM OF THE TROPICAL EAST PACIFIC

BY DAVID J. RAYMOND, STEVEN K. ESBENSEN, CLAYTON PAULSON, MICHAEL GREGG, CHRISTOPHER S. BRETHERTON, WALTER A. PETERSEN, ROBERT CIFELLI, LYNN K. SHAY, CARTER OHLMANN, AND PAQUITA ZUIDEMA

Observations from instrumented ships and airplanes, among other platforms, document the workings of physical processes that are key to improving model simulations of climate in the tropical east Pacific.

Though much progress has been made in the development of coupled ocean–atmosphere models, many discrepancies remain between observations and model results. The tropical east Pacific (i.e., east of about 140°W) is a region in which the performance of coupled models has been problematic (Mechoso et al. 1995), with particular difficulty in the simulation of the seasonal cycle of sea surface temperatures (SSTs) and the associated atmospheric circulations. In this paper and its companion (Bretherton et al. 2004), we describe the objectives and preliminary results of the East Pacific Investigation of Climate Processes in the Coupled Ocean–Atmosphere System 2001 (EPIC2001), a process study designed to document the characteristics of physical processes important to climate models in tropical east Pacific.

In the development of the EPIC2001 field program, the biggest uncertainties in modeling the east Pacific climate system were thought to be due to inadequate representation of certain key physical processes in models, particularly deep cumulus convection, ocean mixing, and stratus region energy balances. The primary purpose of EPIC2001 is to better understand these processes, with the goal of improving climate model performance. In order to provide perspective on these issues, we first describe some of the peculiarities of the regional climate and results of attempts to model it.

Figure 1 shows the central characteristic of the seasonal cycle in the eastern tropical Pacific. In spite of the seasonal passage of the sun north and south across

AFFILIATIONS: RAYMOND—New Mexico Institute of Mining and Technology, Socorro, New Mexico; ESBENSEN AND PAULSON—Oregon State University, Corvallis, Oregon; GREGG AND BRETHERTON—University of Washington, Seattle, Washington; PETERSEN—University of Alabama in Huntsville, Huntsville, Alabama; CIFELLI—Colorado State University, Fort Collins, Colorado; SHAY—University of Miami, Miami, Florida; OHLMANN—University of California, Santa Barbara, Santa Barbara, California; ZUIDEMA—University of Colorado, Boulder, Colorado
CORRESPONDING AUTHOR: David J. Raymond, Physics Department, New Mexico Tech, Socorro, NM 87801
E-mail: raymond@kestrel.nmt.edu
DOI: 10.1175/BAMS-85-9-1341

In final form 8 April 2004

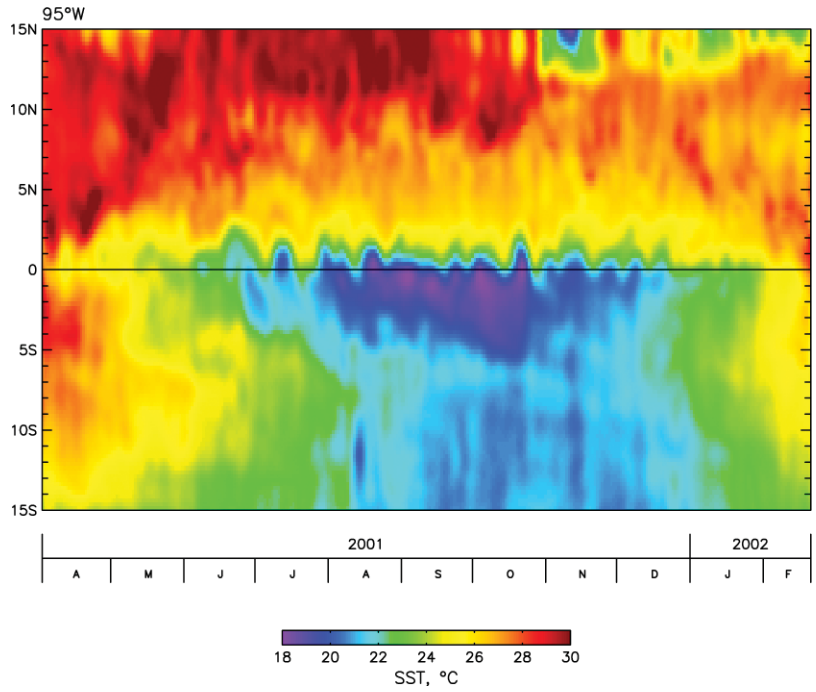

Fig. 1. Satellite SST from the Tropical Rainfall Measurement Mission (TRMM) Microwave Imager (TMI) along 95°W as a function of time and latitude from Apr 2001 through Feb 2002.

the equator, the warmest SSTs remain north of the equator at all times. Only in March and April do the SSTs south of the equator approach those to the north. Deep convection follows warm water (say, in excess of 27°C), though convection is not necessarily maximal over the *warmest* waters. In line with the SST distribution, convection occurs to the south of the equator only during March and April. In this period one sometimes sees a double intertropical convergence zone (ITCZ), with convection both north and south of the equator (Halpern and Hung 2001). During strong El Niño years, when the equatorial water is warm, convection can occur on the equator during this period as well.

A typical problem of climate models is the excessive production of a double ITCZ in this region, contrary to what is observed. This stems partly, but not completely, from a failure to predict accurate SST distributions. It most likely also reflects the inability of models to determine where deep convection will form for given atmospheric conditions. Such a failure is highly detrimental to a model's climate predictions, since it means that large-scale circulations and precipitation patterns (which are intimately related to the distribution and intensity of deep convection) are incorrectly predicted.

Philander et al. (1996) showed that the asymmetry of SSTs between hemispheres in the eastern Pacific (and also the eastern Atlantic) is likely caused by the northwest–southeast orientation of the coastline acting in combination with positive coupled ocean–atmosphere feedback. The orientation of the American coastline means that the southeast trade winds flow more nearly parallel to the coast in the Southern Hemisphere than do the northeast trades in the Northern Hemisphere, resulting in stronger coastal upwelling and colder coastal water to the south. This by itself induces a relatively small latitudinal asymmetry. However, it is sufficient in their modeling work to bias the feedback in the direction of producing warm water to the north and cold water to the south over a broad stretch of the eastern Pacific.

At least two factors contribute to the coupled feedback in models. First, the cross-equatorial flow pattern induced by higher SSTs on one side of the equator exhibits higher average off-equatorial trade winds on the cold side. Low wind speeds occur on the warm side because it is a region of convergence between the opposing northeasterly trade winds and the southwesterly cross-equatorial flow. A stronger tendency toward evaporative cooling of the ocean therefore occurs on the cold side in the model as a result of the stronger trade winds away from the equator, reinforcing the existing SST pattern (Chang and Philander 1994; Xie and Philander 1994; Xie 1994). Second, low stratus clouds tend to develop over cold water, which reflect much of the incoming solar radiation. However, these clouds interfere very little with the loss of energy via thermal radiation, resulting in less radiative heating of the cold water region than in the warm water area. The overall effect of the distribution of evaporation and radiative heating and cooling is thus reinforcement of the preexisting thermal contrast in the model. The resulting atmospheric and oceanic circulations are shown in idealized form in Fig. 2.

Philander et al. (1996) found that the ability of a model to reproduce this equatorially asymmetric structure depends particularly on the correct treatment of low-level stratus clouds in the cold water regions. A proper treatment of stratus-layer energetics and the prediction of the distribution of stratus clouds

are thus crucial to getting both the atmospheric flows and oceanic temperatures right in these areas.

It is clear that the representation of the east Pacific seasonal cycle is rather fragile in existing models, which exhibit large sensitivities to the way in which various processes are represented. The realization that these uncertainties compromise our understanding of this region led to the development of EPIC2001.

An additional problem in the modeling of the east Pacific seasonal cycle is the realistic representation of the effects of disturbances with less than seasonal time scales in climate models. Although climate modeling is concerned with intraseasonal and longer averages of meteorological and oceanographic variables, the shorter time scales can play an important role if their effects rectify onto climatological time scales. Such rectification is important when the short-time-scale disturbances exhibit highly nonlinear behavior.

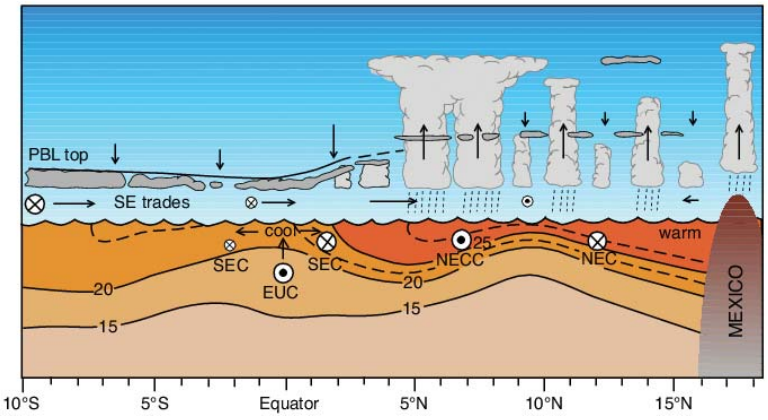

FIG. 2. Idealized cross section through the ITCZ–cold tongue complex in the east Pacific showing the atmospheric meridional circulation, atmospheric boundary layer depth, and the oceanic thermal structure. SEC refers to the South Equatorial Current, NECC to the North Equatorial Countercurrent, and the EUC to the Equatorial Undercurrent. The heavy cloud denotes the position of the ITCZ. Encircled x's (dots) denote westward (eastward) flowing winds or currents.

The surface winds in the east Pacific warm pool, that is, the warm water between about 6°N and the Mexican coast, tend on the average to be light. However, the averaging process hides episodes of strong winds from both the east and the west. Furthermore, intense deep convection appears to be correlated with these episodic strong wind events, possibly as a consequence of the strong surface energy fluxes associated with the strong winds (Raymond et al. 2003). In such a situation climatological average winds in a climate model will not produce climatological average convection unless the wind fluctuations are explicitly or implicitly accounted for in the model.

Rectified nonlinear effects may be important in upper ocean mixing in the east Pacific warm pool as well. If the response of the ocean to surface fluxes is highly nonlinear, then forcing an ocean model with climatological surface fluxes will not result in the climatologically observed mixing. More specifically, if the effects of hurricanes and strong tropical storms are not included somehow in the forcing, the ocean model is not going to get the mixing right, even if the model physics are otherwise perfect. This brings us back to the importance of predicting the distribution of deep convection, not only in seasonal averages, but on a day-to-day basis.

Generally speaking, the seasonal cycle more than a few degrees away from the equator proceeds somewhat independently of the presence or absence of El Niño, which affects the temperature of near-equatorial water most strongly. However, the local airflow across the equator is affected greatly by the SST distribution there (Wallace et al. 1989), which in turn can feed back upon the ocean. When an east–west tongue of cold water is found near the equator, the low-level cross-equatorial flow decouples from the surface over this cold water, leaving a relatively thin layer of air with low wind speeds near the surface. The intense latitudinal shears of the equatorial oceanic current systems give rise to tropical instability waves (TIWs) that cause the sea surface temperature front on the north side of the cold tongue to meander north and south with periods of 20–40 days (see Fig. 1). The SST anomalies associated with these meanders can produce relatively complex three-dimensional flow patterns in the cross-equatorial airflow and constitute another source of intraseasonal variability. These flow patterns and associated surface fluxes were investigated during EPIC2001.

Given the potentially large effects of the rectification of short-time-scale variability on climate, an emerging focus of EPIC2001 has therefore been to document and understand the mechanisms of subseasonal variability in the tropical east Pacific, particularly in the deep convection and in ocean mixing. We focus particular attention on this issue here.

EPIC2001. EPIC was developed under the auspices of the National Oceanic and Atmospheric Administration's (NOAA) Pan-American Climate Studies (PACS) program and later under the U.S. Climate Variability and Predictability (CLIVAR) program to help solve the problems with coupled models in the east Pacific region. As such, it proposed a combination of enhanced monitoring to better elucidate the long-term behavior of the ocean–atmosphere system in this region (see Cronin et al. 2002), and intensive field studies of physical processes known to be poorly represented by model parameterizations in coupled models. The processes of interest include boundary layer and deep convective dynamics in the tropical oceanic atmosphere and mixing across constant density surfaces in the ocean, particularly at the base of the ocean mixed layer.

EPIC2001 was conceived as an intensive process study along and near 95°W. This longitude was chosen to coincide with the TAO mooring array there in order to provide overlap between the process study and long-term monitoring. The "Overview and Implementation Plan" describes EPIC2001 as an intensive field study during September and October of 2001 designed to address the following:

1) the processes that determine the nature of deep convection in and near the ITCZ, including its variability, strength, and location;
2) the evolution of the vertical structure of the atmospheric boundary layer as the surface winds flow northward over the cold tongue and strong SST gradient of the equatorial front;
3) how air–sea coupling affects ocean mixed layer dynamics and SST in the east Pacific warm pool; and
4) the processes in the upper ocean that affect the structure and evolution of the shallow thermocline in this region.

In addition the plan calls for "exploratory observations in the southeastern tropical Pacific during this period [which] will focus on obtaining the dynamical, radiative, and microphysical data needed to evaluate models and parameterizations of boundary layer stratiform cloud formation and evolution and to determine the feedbacks between the ocean and the stratus clouds."

The observational program in the stratus region south of the equator is described elsewhere (Bretherton et al. 2004). In this article we focus on the EPIC2001 observational strategy and selected early results based on observations from the equator northward through the east Pacific ITCZ.

The EPIC2001 field campaign was designed to sample intensively the east Pacific's highly variable meteorological and oceanographic fields over a limited period of time. As Fig. 3 illustrates, EPIC2001 was focused along the 95°W line in order to take advantage of the data from the existing array of Tropical Atmosphere-Ocean (TAO) moorings along this line (McPhaden 1995). Three additional moorings were added to the array for EPIC2001 at 3.5°, 10°, and 12°N, supplementing the seven existing moorings, which stretched from 8°S to 8°N. In addition, all moorings along 95°W were enhanced to measure pressure, rainfall, short- and longwave radiation, upper ocean salinity, and horizontal currents at a 10-m depth.

In addition to the TAO moorings, two aircraft, the National Center for Atmospheric Research's (NCAR) C-130 and one of NOAA's P-3 aircraft, plus two ships, NOAA's R/V *Ron H. Brown* and the National Science Foundation's (NSF's) R/V *New Horizon*, and Galapagos-based soundings, were used to make mea-

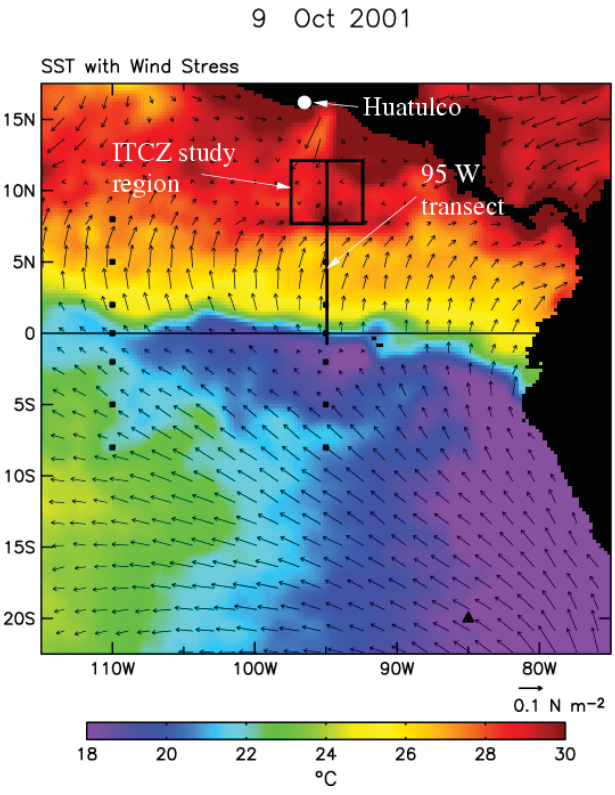

Fig. 3. TMI SST and Quick Scatterometer (QuikSCAT) wind stress measurements in the eastern Pacific for 9 Oct 2001 (day 282). The ITCZ study region and the north–south transect along 95°W are shown, as well as the location of Huatulco, the aircraft base. The black squares are the locations of the standard TAO moorings and the black triangle at 20°S, 85°W indicates the IMET mooring.

surements of the atmosphere and ocean in this region. The aircraft were based from 1 September to 10 October 2001 (Julian day 244 to 283) in Huatulco, Mexico (see Fig. 3), which is the site closest to the 95°W line on the Pacific coast with sufficient airport facilities. The ships spent approximately 3 weeks in the vicinity of 10°N, 95°W, and then traversed the 95°W line to the equator. After a short stop in the Galapagos Islands, the *Ron H. Brown* then proceeded south along 95°W and then to the Woods Hole Oceanographic Institute Improved Meteorological Recorder (IMET) mooring at 20°S, 85°W. Meanwhile the *New Horizon* reversed its track along 95°W and then returned to port.

The strength of the aircraft as a research tool in EPIC2001 was to provide nearly synoptic measurements of spatial variability in both the atmosphere and the ocean. The P-3 carried lower-fuselage and tail radars, the latter with Doppler capability. In addition, it provided in situ wind and thermodynamic measurements, as well as deploying atmospheric dropsondes and expendable ocean probes designed to measure temperature, salinity, and ocean currents. The P-3 was used mainly to do mesoscale mapping of the ITCZ study region from an altitude of 1900 m using its radar, dropsondes, and ocean probes. The C-130 aircraft also deployed dropsondes and ocean probes, the latter being a new capability for this aircraft. In addition to providing in situ wind and thermodynamic data, it was equipped with Scanning Aerosol Backscatter Lidar (SABL) and an extensive array of cloud physics and aerosol instrumentation. High-rate measurements were also available for turbulent flux calculations. Eight C-130 flights were used to document conditions along 95°W, flying a vertical sawtooth pattern in the planetary boundary layer outbound, and dropping dropsondes from high altitude on the return leg. Two other missions were made to study the SST front near the equator, and 10 missions of a variety of types were used to study convection in the ITCZ study region. Table 1 presents information about aircraft missions flown during EPIC2001.

The ship measurements provided some measure of spatial variability on a smaller scale, but excelled in providing temporal continuity in the ITCZ region over a 3-week period. In addition, the ships produced high-spatial-resolution measurements along 95°W, though somewhat aliased in time. The *Ron H. Brown* carried a large array of instrumentation. On the atmospheric side, in situ state and flux measurements were available, as well as the output of a C-band scanning Doppler radar. In addition, a vertically pointing K-band radar and a lidar were on board. Rainfall and aerosol measurements were made as well. Finally, six radiosondes per day were launched from the *Ron H. Brown*. Ocean measurements included standard conductivity–temperature–depth (CTD) casts, turbulent microstructure profiling in order to measure turbulent mixing, and visible radiation flux profiles. The *New Horizon* used a Sea Soar to investigate the small-scale spatial structure of the ocean and also brought to bear a variety of other atmospheric and oceanic measurements.

Table 2 lists the principal investigators involved in the nonstratus region aspects of EPIC2001 and their interests.

MEAN STRUCTURE. Measurements of unprecedented detail were made of the structure of the late northern summer atmosphere and ocean along 95°W in EPIC2001. SSTs during the project were near normal, that is, exhibiting neither El Niño nor La Niña conditions.

Figure 4 shows a cross section of ocean temperatures along the 95°W line for early October 2001. Notice how the warm waters north of 8°N were very shallow as a result of upwelling due to the cyclonic wind stress curl in the ITCZ. This contrasts with the conditions near 4°N, where the thermocline is somewhat deeper, but the mixed layer water near the surface is cooler. The thermocline near the equator is also shallow, reflecting the existence of the equatorial cold tongue.

All of the factors promoting strong ocean–atmosphere coupling are more effective where the oceanic mixed layer and thermocline are shallow. This is because wind-induced upwelling more readily brings cold water to the surface under these conditions. In addition, the thinner oceanic mixed layer results in greater mixed layer temperature tendencies for a given energy imbalance. The east Pacific warm pool is quite shallow, at least compared to equatorial conditions in the western equatorial Pacific, and is thus very sensitive to atmospheric processes.

Figure 5 shows a cross section of the atmosphere below 1800-m elevation along 95°W. The figures in the left column are averages of measurements from the C-130 aircraft over all 95°W flights. For comparison, the corresponding analysis from the National Centers for Environmental Prediction (NCEP) Global Data Assimilation System (GDAS) is shown in the center column. Analyses at 1800 UTC (i.e., quite near the actual flight time) on the days of each flight were averaged to produce the results shown in Fig. 5. The latitudinal and vertical extent of the meridonal flow are similar in the observations and the analysis.

However, the observed winds are somewhat stronger than the analyzed winds over most of the domain, except at low levels near the equator, where they are weaker. The latter effect reflects the detachment of the flow from the surface over the oceanic cold tongue. Significant discrepancies of about 1°C and 2 g kg^{-1} occur in the potential temperature and the water vapor mixing ratio, with the GDAS conditions being generally cooler and drier.

The right column in Fig. 5 shows the September mean along 95°W from a multicentury simulation of the current climate with a state-of-the-art coupled atmosphere–ocean general circulation model, the NCAR Community Climate System Model (CCSM) version 2.0. Because the right column is a climatology, we expect the meridional and vertical gradients of all fields to be somewhat smoothed out. However, there is also a warm SST bias in this model in the east Pacific cold tongue and in the southeast Pacific. The low-level winds are significantly weaker in this model than in observations, but this may be in response to the weaker meridional gradient in the simulated SST distribution.

The flow south of 5°N is typical of the pattern observed throughout the project. The changes in vertical structure of the cross-equatorial boundary layer flow in the atmosphere may have important implications for maintaining the upper ocean structure in the vicinity of the east Pacific cold tongue. Figure 3 shows that the wind stress patterns were dramatically affected by the tendency of the cross-equatorial flow to jump over the cold tongue. The pattern of low wind

TABLE 1. Information about EPIC2001 research flights. The day is computed so that 0000 UTC on 1 Jan 2001 has a value of 1.0. In the mission column, "ITCZ" indicates a study in the ITCZ study region using either the P-3 or the C-130 or both, "95°W" indicates a C-130 traverse of 95°W, and "SST" indicates a C-130 study of the SST front near the equator. The names in capital letters under Comments indicate tropical storm passages. IRIS was an Atlantic tropical storm, the remnants of which passed overhead. The P-3 flight 0109281 was aborted due to engine failure. Flight 0109211 was an operational flight into Tropical Storm Juliette. Reproduced from Raymond et al. (2003).

Day	Date	Mission	P-3	C-130	Comment
246	3 Sep	1 - ITCZ	0109031	RF01	
248	5	2 - ITCZ	0109051	RF02	
250	7	3 - 95°W	0109071	RF03	
252	9	4 - ITCZ	0109091	RF04	IVO
256	13	5 - ITCZ	0109131	RF05	
257	14	6 - 95°W		RF06	
259	16	7 - ITCZ	0109161	RF07	KIKO South
262	19	8 - 95°W		RF08	
263	20	9 - ITCZ	0109201	RF09	JULIETTE East
264	21	Operational	0109211		JULIETTE
266	23	10 - 95°W		RF10	JULIETTE West
268	25	11 - 95°W		RF11	
271	28	12 - ITCZ	(0109281)	RF12	LORENA West
272	29	13 - ITCZ		RF13	LORENA West
275	2 Oct	14 - 95°W		RF14	
276	3	15 - ITCZ/SST	0110031	RF15	
278	5	16 - ITCZ/SST	0110051	RF16	
279	6	17 - ITCZ	0110061	RF17	
280	7	18 - ITCZ	0110071		
282	9	19 - 95°W		RF18	IRIS over Huatulco
283	10	20 - 95°W		RF19	

stress over the cold tongue and high wind stress to the north of the SST front can result in very large values of wind stress curl and divergence in the vicinity of the SST front (Chelton et al. 2001). As the first sidebar shows, the SST front can be exceedingly sharp, with large cross-front differences in air–sea fluxes.

Solar radiation and its vertical divergence in the water column are crucial to the energy balance of the ocean mixed layer. The attenuation of solar radiation in the upper ocean is primarily regulated by upper-ocean chlorophyll biomass, which can be highly varying in both time and space (Lewis et al. 1990; Ohlmann et al. 1998; McClain et al. 2002). In-water solar flux profiles to 100 m were recorded from the *Ron H. Brown* while on station near 10°N, and along the 95°W transect. In addition, water samples were collected daily at eight depths and analyzed for chlorophyll *a* concentration using Turner fluorometry. The irradiance data are sufficient for quantifying available solar energy at the sea surface and computing the fraction of available surface irradiance that exists at depth, or solar transmission. The chlorophyll data make it possible to address biologically induced changes in transmission. Observed solar transmission was significantly larger than values estimated from regional Jerlov water-type parameterizations. For example, the average observed transmission at a 10-m depth was 25% of the surface irradiance compared to 11% estimated with the standard Jerlov parameterization. This discrepancy corresponds to an absolute solar flux difference near 20 W m^{-2} and a radiant heating rate difference of more than 1.2°C $month^{-1}$ for the layer (assuming a climatological surface flux of

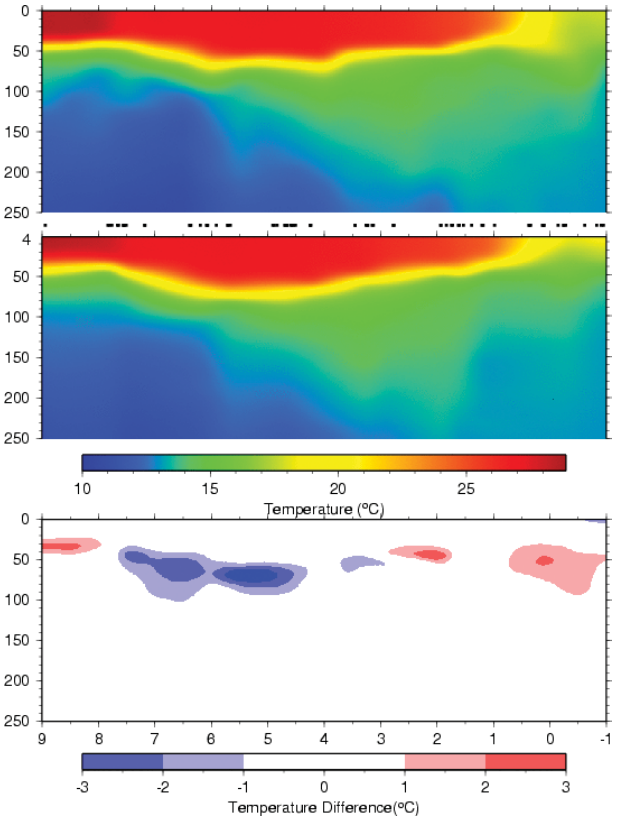

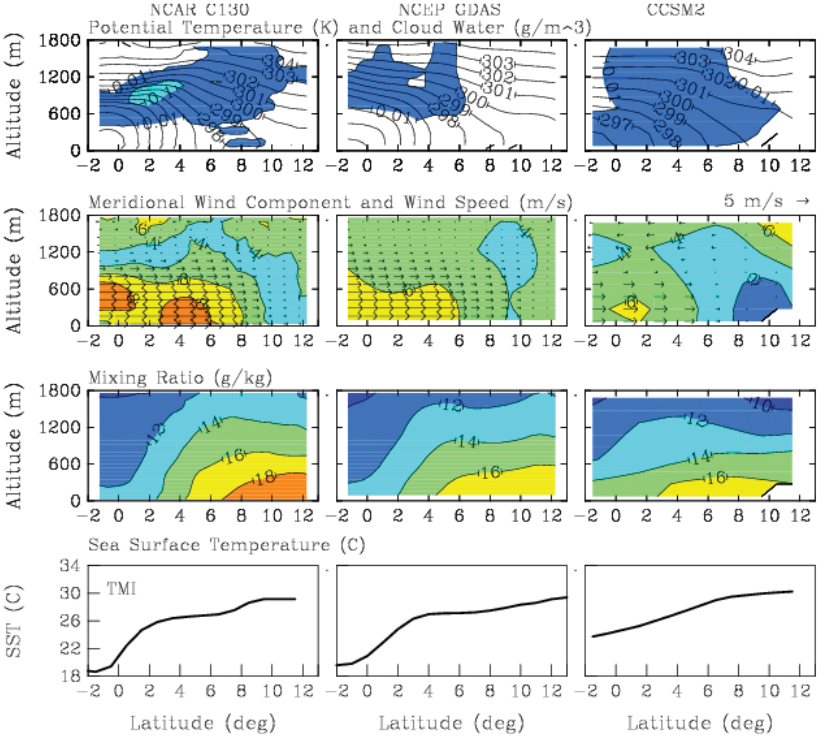

FIG. 4 (figure at top right). Ocean temperature as a function of depth and latitude along 95°W from (top) *Ron Brown* measurements (1–4 Oct, or days 274–277) and (middle) C-130 expendable ocean probe measurements (2, 9, 10 Oct, or days 275, 282, and 283). The black dots between the panels indicate the locations of ocean probe deployments from the C-130. The bottom panel shows the difference between the two.

FIG. 5 (figure at right). Cross section along 95°W of potential temperature, cloud water, meridional wind, mixing ratio, and SST averaged over the eight C-130 flights along 95°W. (left) From the C-130 aircraft and the TMI sensor on the TRMM satellite. (center) NCEP GDAS analysis. (right) NCAR CCSM coupled model mean September conditions.

THE EQUATORIAL SST FRONT

SST gradients on the order of a few degrees Celsius in 10 km are frequently observed across coastal ocean fronts. However, EPIC2001 oceanographers aboard the R/V *New Horizon* did not expect to find SST gradients of this magnitude across the front on the northern boundary of the equatorial cold tongue. Surprisingly, the equatorial SST front was not only extremely sharp, but was south of the equator. Large changes in surface sensible and latent heat flux and wind stress were observed as the northward-flowing air crossed the front.

Figure SB1 shows time–space series of SST, air temperature and sensible heat flux measured while the R/V *New Horizon* steamed along 95°W at 4 m s^{-1}. The ship first steamed south, reaching 1°S on 6 October (day 279), and then turned north, continuing at the same speed. The front south of the equator was very sharp when crossed the second time from south to north; SST changed 1.7°C over a distance of 700 m. Air and surface temperature were nearly the same south of the front over the cold tongue, indicating that the lower atmosphere stratification was near neutral. In contrast, SST exceeded air temperature by about 2°C north of the front,indicating unstable stratification. Sensible heat flux over the cold tongue was near zero, but reached 40 W m^{-2} north of the front.

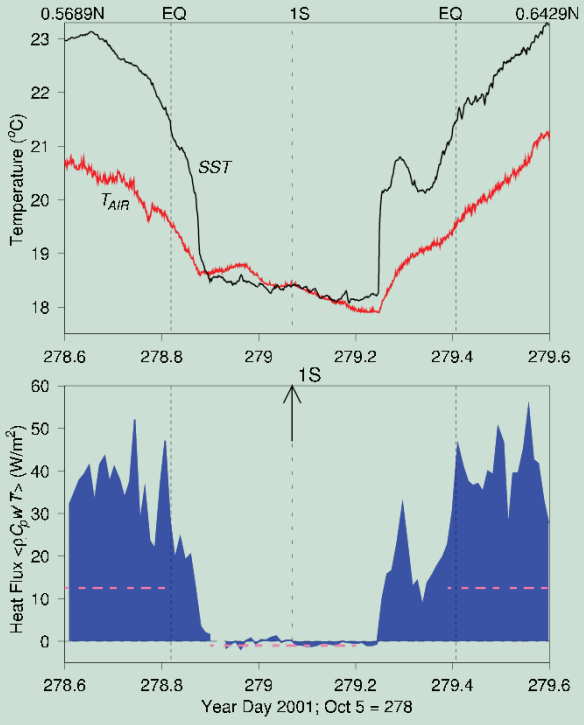

FIG. SB1. (top) SST and air temperature and (bottom) surface sensible heat flux from the ship R/V *New Horizon* crossing the equatorial SST front.

170 W m^{-2}). The solar transmission data have provided necessary information for upper-ocean heat budget research, and have validated an improved solar transmission parameterization for use in climate models (Ohlmann 2003).

EAST PACIFIC VARIABILITY. Subseasonal variability in the meteorological and oceanographic fields north of about 5°N is very large, and extends from diurnal (see sidebar 2) to intraseasonal time scales. Figure 6 shows a longitude–time plot for the EPIC field phase of the geosynchronous satellite infrared brightness temperature averaged over 8°–12°N. Deep convection, as indicated by low brightness temperatures, is very sporadic, and tends to be concentrated in westward-moving bursts. These bursts have been identified with African easterly waves that have

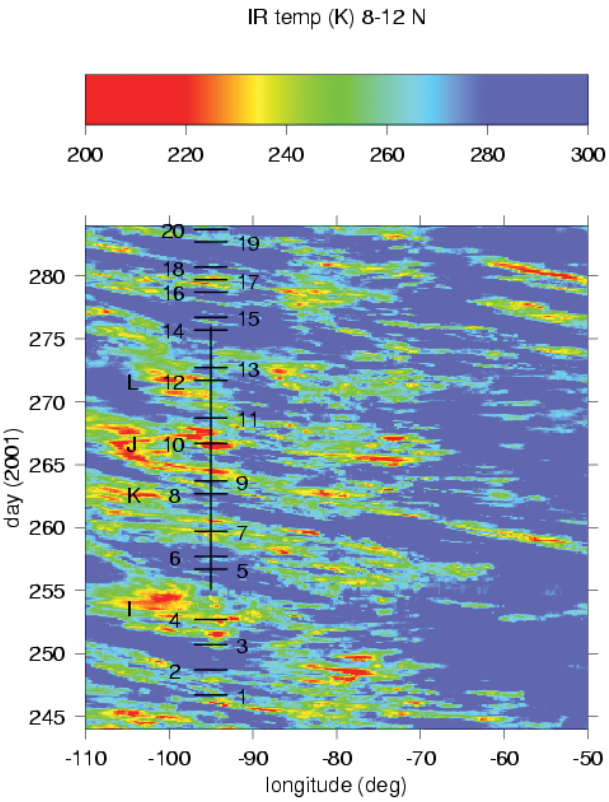

FIG. 6. Longitude–time section of infrared brightness temperature from Geostationary Operational Environmental Satellite (GOES), averaged over 8°–12°N during the EPIC field phase. The horizontal lines and numbers show the timing of EPIC aircraft missions and the vertical line shows the time during which the ship *Ron Brown* was present at 10°N, 95°W. The letters indicate the east Pacific Tropical Storms Ivo, Juliette, Kiko, and Lorena or their precursors, which developed during EPIC. (Kiko appears before Juliette because it was not named until it had reached a point much further west.)

survived the passage across the Atlantic and Central America (see Avila et al. 2003). It is not clear whether all such disturbances truly originate in Africa—it is easier to make such identifications in retrospect than in real time, as we discovered during the field program—but some can be traced continuously back to Africa in various fields. What is clear is that many of them intensify into tropical storms once they reach the eastern Pacific. As Fig. 6 indicates, four waves became tropical storms during the period of the experiment.

Figure 7 shows the results of compositing radiosonde soundings taken between 13 September and 2 October (day 256–275) at 10°N, 95°W from the ship *Ron H. Brown*. The composite is constructed by classifying soundings relative to the phase of westward-moving wave disturbances. The major categories are trough (T), ridge (R), northerly flow in the lower troposphere (N), and southerly flow there (S). The trough occurs at the transition from northerly to southerly flow, and the ridge at the reverse transition. This work is described in detail by Petersen et al. (2003).

Petersen et al. (2003) found that convection covered less area but was more vertically developed in the northerly phase, whereas the convection was more widespread but less vertically developed in the trough and southerly phases. Convective rainfall dominated all the phases, but there was a larger percentage of stratiform rain in the trough and southerly phase. As Fig. 7 shows, the troposphere was more humid in the southerly flow regime than in the northerly regime. Convective available potential energy (CAPE) was less in the southerly flow than in the northerly flow due to reduced values of wet-bulb potential temperature at the surface (Petersen et al. 2003). The effect of temperature perturbations aloft on CAPE was relatively minor.

Careful examination of soundings south of about 10°N indicates that a northerly return flow often exists above about 1-km elevation. This flow is highly variable from day to day, and seems to be strongest

THE DIURNAL CYCLE IN CLOUDS AND PRECIPITATION

A strong diurnal cycle was observed at the *Ron Brown*, with a broad 0300 LT–noon maximum and 1500 LT–midnight minimum in precipitation and cloudiness. This is evident in a variety of data sources, shown in Fig. SB2: cloud radar data, the precipitation radar data averaged over 30- and 100-km diameter circles, shipboard rain gauge data, and the TAO buoy rain gauge data (Dr. Y. Serra 2003, personal communication). The *Ron Brown* precipitation measurements show a strong 0300 LT peak, but the precipitation peak at the TAO buoy at 10°N, 95°W occurs at 0600 LT. These differences in the time of peak precipitation may reflect slightly different spatial sampling of the westward-propagating precipitation systems. A second glance at Fig. SB2 reveals an intriguing association between the rainfall estimates and the overlying cloudiness distribution: while the early morning precipitation peak corresponds well with a cloudiness maximum occurring within the boundary layer, the late-morning precipitation is associated with two cloudiness peaks that are above the freezing level. Each distinct cloudiness population manifests its own diurnal variation, with the highest-altitude cloudiness amount peaking the latest, after sunrise. Further study will be required to understand the cloudiness vertical distribution and its relationship to the convection.

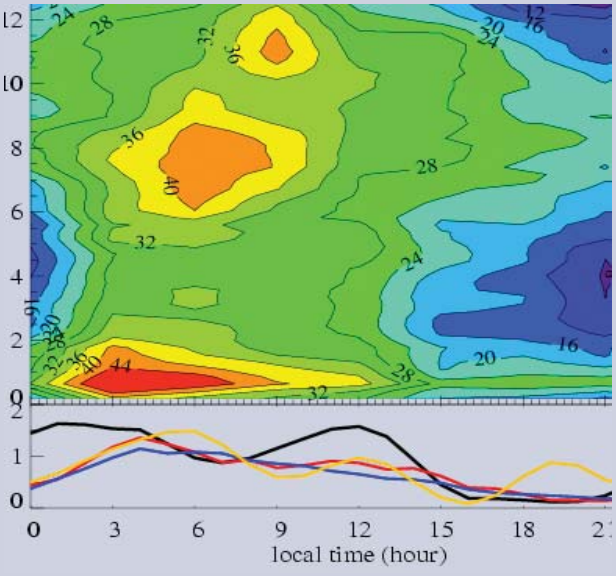

Fig. SB2. (top) The *Ron Brown* mean diurnal cycle of cloud radar echo distribution (> –40 dBZ) as a percentage of the total number of cloud radar scans occurring during each 3-h time period centered upon the labeled hours, spanning 10 Sep–1 Oct (day 253–274). (bottom) The mean rainfall diurnal cycle from rain gauges at the *Ron Brown* (black line), the C-band radar rainfall estimates within a circle of 30- (red line) and 100-km (blue line) diameter centered on the *Ron Brown*, and the TAO buoy rain gauge (orange line). The original time series span approximately the same time interval, and are smoothed to an hourly time resolution. The precipitation radar rainfall estimates are averaged hourly and the rain gauge hourly averages are formed from 3-hourly time periods centered upon the hour.

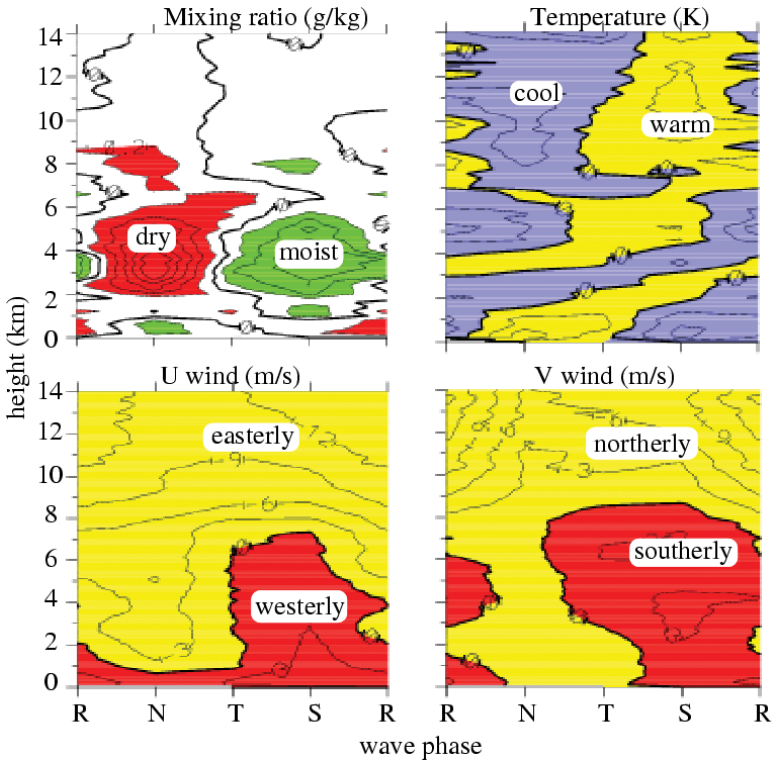

FIG. 7. Composite of *Ron Brown* soundings at 10°N, 95°W classified according to easterly wave phase. Phases are as follows: N is northerly regime, T is trough, S is southerly regime, R is ridge, with time advancing from left to right. The temperature and mixing ratio plots are perturbations from the mean state.

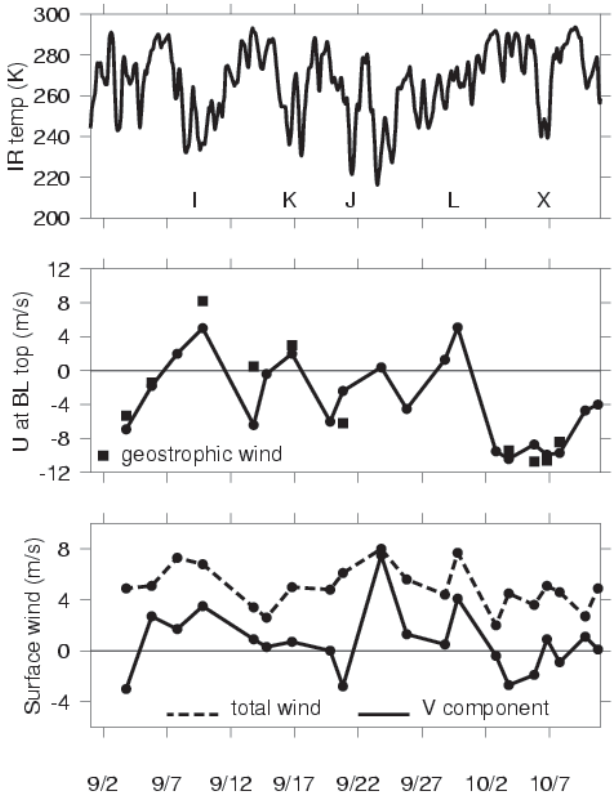

on days with weak or nonexistent deep convection in the ITCZ. However, it is also detectable in the time-averaged state, indicating that the Hadley circulation in the region consists of the superposition of a shallow and a deep cell (Zhang et al. 2004).

A major goal of EPIC2001 is to ferret out the mechanisms controlling deep convection in the east Pacific ITCZ. Significant progress is being made on this topic. Raymond et al. (2003) found that surface moist entropy (or total heat) fluxes are a major predictor of deep convection in the region, as is a measure of the convective inhibition to lifting of a deep (≈ 1 km) layer of near-surface air. Variations in these two factors together account for 2/3 of the variance in satellite infrared brightness temperature (a measure of deep convection) in the 4° x 4° box centered on 10°N, 95°W.

Figure 8 shows a time series of the infrared brightness temperature and winds at the surface and above the boundary layer top (≈ 1.5 km) in the box 8°–12°N, 93°–97°W for the period of the EPIC2001 project. The correlation between westerly winds at the boundary layer top and the passage of tropical storm precursors is quite striking. In contrast, the last 10 days of the project, in which no tropical storms occurred, exhibited strong easterlies at this level.

This result is in agreement with those of Molinari et al. (1997) and Maloney and Hartmann (2000, 2001a,b), who show that east Pacific tropical cyclo-

FIG. 8. Time series for EPIC. (top) The GOES infrared brightness temperature averaged over the ITCZ study region. The letters I, J, K, and L indicate the passage of tropical storm precursors by 95°W. The letter X indicates convection apparently associated with a strong easterly jet. (middle) The average zonal wind between 810 and 830 hPa from dropsondes in the ITCZ study region. The box symbols show the geostrophic zonal wind near 810 hPa from P-3 in situ pressure measurements. (bottom) The meridional and total wind averaged over the ITCZ study region near the surface. Dropsonde winds were averaged over 980–1000 hPa to obtain these results.

genesis is highly correlated with lower-tropospheric westerlies there. These authors attribute the westerlies to the Madden–Julian oscillation (MJO; see Madden and Julian 1994); other types of disturbances such as equatorial Kelvin waves (Straub and Kiladis 2002) can also produce transient westerlies in this region. Wind variations at 850 hPa appear to be connected to coherent wind signals propagating into the region from the west, with the transition to easterlies near 1 October (day 274) possibly being associated with the end of the active MJO phase (E. Maloney 2002, personal communication).

In any case, strong variability in the zonal flow in the lower troposphere exists in the east Pacific, and westerlies are significantly correlated to deep convection in this region, and in particular to tropical cyclogenesis. This variability has a component with a longer time scale than the variability associated with the passage of easterly waves, and it tends to modulate the intensification of these waves into tropical storms.

Significant mesoscale oceanic variability in the east Pacific warm pool occurs as well. Expendable ocean probes (current profilers, conductivity–temperature–depth profilers, and bathythermographs) were deployed in a grid pattern over the ITCZ study region by the P-3 aircraft during EPIC2001. These data were objectively analyzed over this region. Figure 9 shows changes over a few weeks in patterns of ocean mixed layer current, temperature, and thickness in the ITCZ study region. Temperature variations up to 3°C and mixed layer thickness variations between 20 and 45 m were found between a westward-moving warm region and the surrounding waters. The flow pattern and temperature structure are consistent with westward-propagating oceanic Rossby waves (Hanson and Maul 1991). These ocean temperature variations may be sufficient to affect the patterns of deep convection in the region; this requires further study.

Figure 10 shows *Ron H. Brown* cruise mean ocean profiles at 10°N of potential temperature, potential density, salinity, and dissolved oxygen, as well as current profiles. Water density is lower above the thermocline as a result of both higher temperatures and

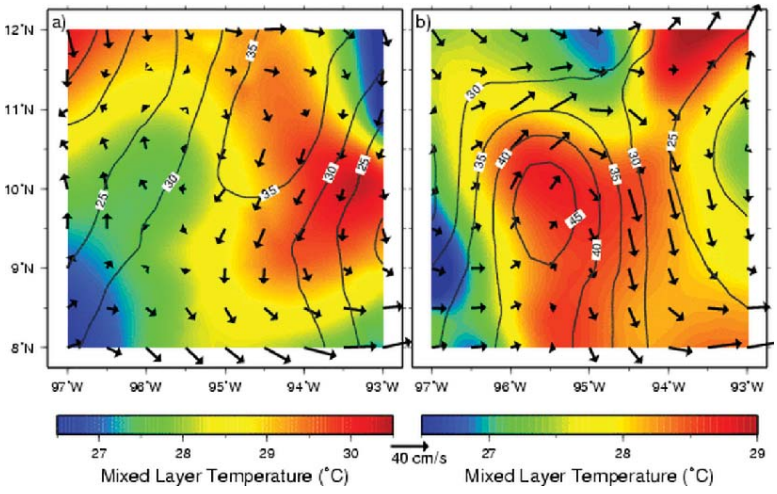

FIG. 9. Objectively analyzed mixed layer temperatures (colors), depths (m, contours), and integrated mixed layer currents (arrows) composited from (a) mid-Sep (13, 16, 20 Sep or days 256, 259, and 263) and (b) early Oct (3, 5, 6, 7 Oct or days 276, 278, 279, 280) over the warm pool of the eastern Pacific Ocean. Data were obtained from expendable ocean probes deployed from the P-3 during the ITCZ flights.

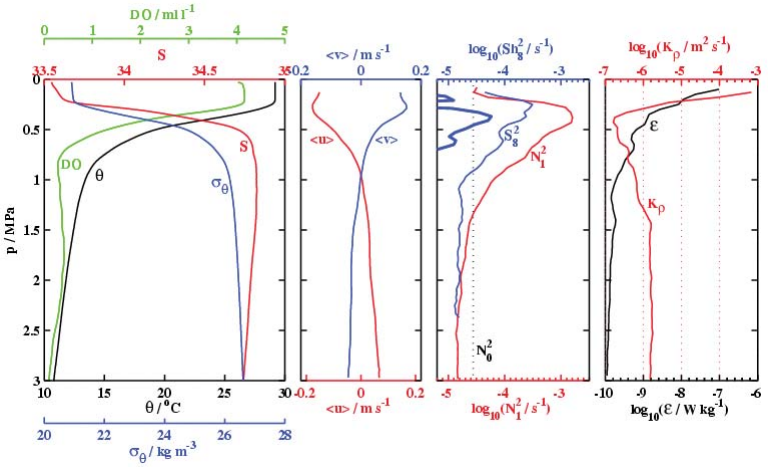

FIG. 10. Cruise-average profiles near 10°N, 95°W for ocean microstructure measurements from the ship *Ron Brown*. First panel, potential temperature θ, salinity S, potential density σ_θ, and dissolved oxygen DO. The second panel, mean current profiles. Third panel, the thick line is the square of the mean shear. The thin lines show the squares of the shear fluctuations and the mean Brunt frequency N_0. Fourth panel, the energy dissipation rate E and the diapycnal diffusivity K_ρ. Note that 1 MPa ≈ 100 m in depth.

lower salinity. Also shown are station-average velocity profiles showing that the surface mixed layer was moving about 0.15 m s^{-1} to the northwest, while the water below the pycnocline was more sluggish. The eddy component of shear S clearly dominates the mean shear at all levels. The third panel compares the stratification (Brunt–Väisälä frequency squared N^2) and shear variance. Most of the shear variance was contributed by internal waves, and the results presented represent a significant underestimate owing to the limited vertical resolution of the shipboard acoustic Doppler current profiler (ADCP). Considering only the contribution from the mean flow gives strong dynamic stability ($S^2 << N^2$), but including the fluctuations shows that the flow was often closer to shear instability.

The fourth panel of Fig. 10 shows the turbulent dissipation rate, E, and the diapycnal eddy diffusivity, which is derived from it as $K_\rho = 0.2EN^{-2}$. The dissipation rate is measured with small airfoil probes on the microstructure profilers and interpreted as diapycnal diffusivity by assuming that turbulent production and dissipation are in local balance. The technique has been used for 20 yr and verified by comparisons with the rate at which streaks of injected tracers thicken. As Fig. 10 shows, the diapycnal eddy diffusivity K_ρ is large in and just below the ocean mixed layer, which means that significant entrainment through the bottom of the mixed layer is occurring. However, K_ρ goes essentially to zero in the region of strong static stability in the thermocline. Below the thermocline the eddy diffusivity is caused primarily by shear instability induced by transient, near-inertial wave motions, with the effects of ambient shear being much weaker. These waves are generated by wind stress forcing at the surface. Initially the shear motions below the thermocline were very weak, but they intensified after 23 September 2001 (day 266) as energy from a strong storm (a peripheral disturbance associated with Tropical Storm Juliette) worked its way downward. The accompanying mixing accounted for most of what little mixing there was between depths of 100–200 m. Mixing in the thermocline, particularly at the base of the surface mixed layer, appears to respond mostly to wind stress.

It thus appears that oceanic mixing below the mixed layer occurs when the shear in near-inertial waves is strong enough to cause the local Richardson number to drop below the critical value for shear instability. Therefore, oceanic mixing should be a highly nonlinear process, with no mixing occurring when wave-induced shear does not cross this threshold. Given this reasoning, the strongest atmospheric disturbances are likely to cause an inordinately large fraction of the total mixing. Profound errors could occur in climate models, which fail to take this into account.

IMPLICATIONS FOR CLIMATE MODELS. One of the ultimate goals of EPIC2001 is to improve the performance of climate models in the eastern tropical Pacific through comparison with observations and improvements in representation of the key physical processes. Through careful validation of model performance and better understanding of model errors through data analysis and process modeling, there is potential for significant improvement in the representation of the key physical processes in simulating eastern Pacific climate and its variability.

As an example, the panels on the right of Fig. 5 illustrate the present status of a state-of-the-art atmospheric data assimilation system and a coupled climate model in representing the observed cross-equatorial boundary layer. The NCEP GDAS analysis reproduces many of the observed features of the C-130 cross section, but as noted above, there are also some significant discrepancies that may have important implications for simulating air–sea interaction in the cross-equatorial ITCZ inflow. The CCSM simulation is farther from observations, but to be fair, includes a composite of both El Niño and La Niña conditions, which could bias the SST distribution from the actual conditions during EPIC2001.

The analysis of EPIC2001 data is still in an early stage. It is clear however that the field program succeeded in acquiring an ocean–atmosphere dataset along 95°W that will be very useful for improving the representation of physical processes in climate models. The aircraft program provided an unprecedented look at the details of the cross-equatorial flow from the cold tongue to the warm pool region along 95°W. The extended record of ocean–atmosphere observations in the ITCZ region, with its shallow oceanic mixed layer and strong atmospheric disturbances, provides an interesting contrast to conditions observed in the Tropical Ocean Global Atmosphere Coupled Ocean–Atmosphere Response Experiment (TOGA COARE; Webster and Lukas 1992), the Joint Air–Sea Interaction Experiment (JASMINE; Webster et al. 2002), and other field programs, and presents an opportunity to test and improve mixing and convective parameterizations for climate models in a much different environment. All EPIC2001 observations were made in the context of enhanced monitoring of the eastern Pacific by satellites, ships, and moored buoys. As results emerge from this and other

Table 2. List of principal investigators involved in the ITCZ, cross-equatorial flow, and warm pool/cold tongue oceanography aspects of EPIC2001.

Principal investigator	Institution	Subject
Bates, J.	NOAA/CDC	Real-time forecasts
Bond, N.	NOAA/PMEL	Cross-equatorial flow (turbulence)
Bretherton, C.	University of Washington	Cross-equatorial flow (LES, data synthesis)
Cronin, M.	NOAA/PMEL	TAO moorings
Esbensen, S.	Oregon State University	Cross-equatorial flow (NCEP comparison)
Fairall, C.	NOAA/ETL	Shipborne remote sensing, surface fluxes
Gregg, M.	University of Washington	Turbulent ocean microstructure
Ohlmann, C.	University of California, Santa Barbara	Ocean absorption of sunlight
Paulson, C.	Oregon State University	Ocean measurements
Petersen, W. Cifelli, R., and Rutledge, S.	Colorado State University	Ship C-band radar, soundings
Raga, G., and Baumgardner, D.	Universidad Nacional Autónoma de Mexico (Mexico)	C-130 cloud and aerosol physics
Raymond, D.	New Mexico Tech	Deep convection, ITCZ
Rudnick, D.	University of California, San Diego/Scripps	Ocean measurements (Sea Soar)
Shay, L.	Rosenstiel School of Marine and Atmospheric Science, University of Miami	Mesoscale ocean variability (ocean probes)
Zehnder, J. and Molinari, J.	Arizona State University and University at Albany, State University of New York	Easterly waves, ITCZ
Zhang, C.	Rosenstiel School of Marine and Atmospheric Science, University of Miami	Cross-equatorial flow, ITCZ (dropsondes)

process studies in the region, we look forward to making significant progress in understanding the complex climate system of the eastern Pacific Ocean.

For information on data availability and other supplementary material, the reader is encouraged to visit the Web site www.physics.nmt.edu/~raymond/epic2001/epicsupplement/readme.html.

ACKNOWLEDGMENTS. Principal investigators are listed in Table 2. We thank Chris Fairall for his key role in the *Ron H. Brown* operations and observations, the Colorado State University crew for their work on the *Ron H. Brown* radar and sounding observations, Dan Rudnick for the Sea Soar observations, Yolande Serra for her analysis of TAO mooring rainfall data, and Hua-Lu Pan for collaboration on C-130 observation and NCEP analysis intercomparisons. Dudley Chelton and Michael Schlax produced the figure of QuikSCAT wind stresses and TMI SST. Chidong Zhang, Joe Zehnder, Graciela Raga, Darrel Baumgardner, Nick Bond, and John Bates were involved in aspects of EPIC2001 not reported here, but helped greatly in stimulating a lively exchange of ideas. The NSF and NOAA ship and aircraft crews, the UCAR JOSS team, and the staff of the Centro de Ciencias de la Atmósfera of the Universidad Nacional Autónoma de México were indispensable to the successful completion of this project. We are also grateful to our colleagues at the Ecuadorian Instituto Nacional de Meteorología y Hidrología for their assistance with operations in the Galápagos. Beverly Davis put together the electronic supplement for the paper. This work was supported by the Consejo Nacional de Ciencia y Tecnología of Mexico, the National Science Foundation, and the National Oceanic and Atmospheric Administration under the auspices of the U.S. CLIVAR program.

REFERENCES

Avila, L. A., R. J. Pasch, J. L. Beven, J. L. Franklin, M. B. Lawrence, S. R. Stewart, and J.-G. Jiing, 2003: Eastern North Pacific hurricane season of 2001. *Mon. Wea. Rev.,* **131,** 249-262.

Bretherton, C. S., T. Uttal, C. W. Fairall, S. Yuter, R. Weller, D. Baumgardner, K. Comstock, and R. Wood, 2004: The EPIC 2001 stratocumulus study. *Bull. Amer. Meteor. Soc.,* **85,** 967–977.

Chang, P., and S. G. H. Philander, 1994: A coupled ocean–atmosphere instability of relevance to seasonal cycle. *J. Atmos. Sci.,* **51,** 3627–3648.

Chelton, D. B., and Coauthors, 2001: Observations of coupling between surface wind stress and sea surface temperature in the eastern tropical Pacific. *J. Climate,* **14,** 1479–1498.

Cronin, M. F., N. Bond, C. Fairall, J. Hare, M. J. McPhaden, and R. A. Weller, 2002: Enhanced oceanic and atmospheric monitoring underway in the eastern Pacific. *EOS Trans. Amer. Geophys. Union,* **83,** 205–211.

Halpern, D., and C.-W. Hung, 2001: Satellite observations of the southeast Pacific intertropical convergence zone during 1993–1998. *J. Geophys. Res.,* **106,** 28 107–28 112.

Hanson, D. V., and G. A. Maul, 1991: Anticyclonic rings in the eastern tropical Pacific ocean. *J. Geophys. Res.,* **96,** 6965–6979.

Lewis, M. R., M.-E. Carr, G. C. Feldman, W. Esaias, and C. McClain, 1990: Influence of penetrating solar radiation on the heat budget of the equatorial Pacific Ocean. *Nature,* **347,** 543–545.

Madden, R. A., and P. R. Julian, 1994: Observations of the 40–50-day tropical oscillation—A review. *Mon. Wea. Rev.,* **122,** 814–837.

Maloney, E. D., and D. L. Hartmann, 2000: Modulation of eastern North Pacific hurricanes by the Madden–Julian oscillation. *J. Climate,* **13,** 1451–1460.

——, and ——, 2001a: The Madden–Julian oscillation, barotropic dynamics, and North Pacific tropical cyclone formation. Part I: Observations. *J. Atmos. Sci.,* **58,** 2545–2558.

——, and ——, 2001b: The Madden–Julian oscillation, barotropic dynamics, and North Pacific tropical cyclone formation. Part II: Stochastic barotropic modeling. *J. Atmos. Sci.,* **58,** 2559–2570.

McClain, C. R., J. R. Christian, S. R. Signorini, M. R. Lewis, I. Asanuma, D. Turk, and C. Dupouy-Douchement, 2002: Satellite ocean-color observations of the tropical Pacific Ocean. *Deep-Sea Res. II,* **49,** 2533–2560.

McPhaden, M. J., 1995: The tropical atmosphere ocean array is completed. *Bull. Amer. Meteor. Soc.,* **76,** 739–741.

Mechoso, C. R., and Coauthors, 1995: The seasonal cycle over the tropical Pacific in coupled ocean–atmosphere general circulation models. *Mon. Wea. Rev.,* **123,** 2825–2838.

Molinari, J., D. Knight, M. Dickinson, D. Vollaro, and S. Skubis, 1997: Potential vorticity, easterly waves, and eastern Pacific tropical cyclogenesis. *Mon. Wea. Rev.,* **125,** 2699–2708.

Ohlmann, J. C., 2003: Ocean radiant heating in climate models. *J. Climate,* **16,** 1337–1351.

——, D. A. Siegel, and L. Washburn, 1998: Radiant heating of the western equatorial Pacific during TOGA-COARE. *J. Geophys. Res.,* **103,** 5379–5395.

Petersen, W. A., R. Cifelli, D. J. Boccippio, S. A. Rutledge, and C. Fairall, 2003: Convection and easterly wave structures observed in the eastern Pacific warm pool during EPIC-2001. *J. Atmos. Sci.,* **60,** 1754–1773.

Philander, S. G. H., D. Gu, D. Halpern, G. Lambert, N. C. Lau, T. Li, and R. C. Pacanowski, 1996: Why the ITCZ is mostly north of the equator. *J. Climate,* **9,** 2958–2972.

Raymond, D. J., G. B. Raga, C. S. Bretherton, J. Molinari, C. López-Carrillo, and Ž. Fuchs, 2003: Convective forcing in the intertropical convergence zone of the east Pacific. *J. Atmos. Sci.,* **60,** 2064–2082.

Straub, K. H., and G. N. Kiladis, 2002: Observations of a convectively coupled Kelvin wave in the eastern Pacific ITCZ. *J. Atmos. Sci.,* **59,** 30–53.

Wallace, J. M., T. P. Mitchell, and C. Deser, 1989: The influence of sea-surface temperature on surface wind in the eastern equatorial Pacific: Seasonal and interannual variability. *J. Climate,* **2,** 1492–1499.

Webster, P. J., and R. Lukas, 1992: TOGA COARE: The TOGA Coupled Ocean–Atmosphere Response Experiment. *Bull. Amer. Meteor. Soc.,* **73,** 1377–1416.

——, and Coauthors, 2002: The JASMINE pilot study. *Bull. Amer. Meteor. Soc.,* **83,** 1603–1630.

Xie, S.-P., 1994: On the genesis of the equatorial annual cycle. *J. Climate,* **7,** 2008–2013.

——, and S. G. H. Philander, 1994: A coupled ocean–atmosphere model of relevance to the ITCZ in the eastern Pacific. *Tellus,* **46,** 340–350.

Zhang, C., M. McGauley, and N. A. Bond, 2004: Shallow meridional circulation in the tropical eastern Pacific. *J. Climate,* **17,** 133–139.